| OF |
AD
A054603

END
DATE
FILMED
7 -78
DDC

MICROCOPY RESOLUTION TEST CHART

NATIONAL BUREAU OF STANDARDS 1963-A

FOR FURTHER TRAN

AD A054603

DDC FILE COPY
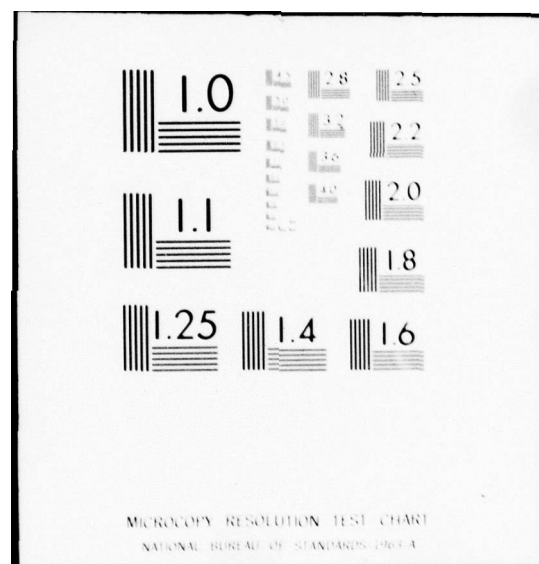
DOCUMENT CONTROL DATA - R & D

(Security classification of title, body of abstract and indexing annotation must be entered when the overall report is classified)

1. ORIGINATING ACTIVITY (Corporate author)	2a. REPORT SECURITY CLASSIFICATION
University of Pennsylvania	Unclassified
	2b. GROUP

3. REPORT TITLE

Intergranular Fracture in 4340-Type Steels; Effects of Impurities and Hydrogen.

4. DESCRIPTIVE NOTES (Type of report and inclusive dates)

Final report for period 8 December 1975 — 7 December 1976,

5. AUTHOR(S) (First name, middle initial, last name)

Samir K. Banerji, Charles J. McMahon, Jr. and Howard C. Feng

6. REPORT DATE	7a. TOTAL NO. OF PAGES	7b. NO. OF REFS
3 January 1977 60 p.	58	27

8a. CONTRACT OR GRANT NO.	9a. ORIGINATOR'S REPORT NUMBER(S)
N00019-76-0298	
b. PROJECT NO.	
c.	9b. OTHER REPORT NO(S) (Any other numbers that may be assigned this report)
d.	

10. DISTRIBUTION STATEMENT

Approved for public release, distribution unlimited

DDC
JUN 2 1978
RECEIVED
F

11. SUPPLEMENTARY NOTES	12. SPONSORING MILITARY ACTIVITY
N00019-76-C-0298, N00019-75-C-0125	U. S. Naval Air Systems Command Headquarters, Washington, D. C.

13. ABSTRACT

A study has been made of the conditions which lead to intergranular brittle fracture in 4340-type steels at an ultra high yield strength level (200 ksi, 1380 MPa) in both an ambient environment and gaseous hydrogen. By means of Charpy impact tests on commercial and high purity steels, and by Auger electron spectroscopy of fracture surfaces, it is shown that one-step temper embrittlement (OSTE or "500°F embrittlement"), and low-K intergranular cracking in gaseous hydrogen are the result of segregation of P to prior austenite grain boundaries. Segregation of N also contributes to OSTE. Most, if not all, segregation apparently occurs during austenitization, rather than during tempering. Elimination of impurity effects by use of a high purity NiCrMoC steel results in an increase in K_{th} for hydrogen-induced cracking by about a factor of five (to the range 130-140 $MNm^{-3/2}$). These observations are discussed in terms of our understanding of the mechanisms of OSTE and hydrogen-assisted cracking.

DD FORM 1473 (PAGE 1)
1 NOV 55

S/N 0101-807-6811

410408

KEY WORDS	LINK A		LINK B		LINK C	
	ROLE	WT	ROLE	WT	ROLE	WT
1. intergranular brittle fracture						
2. 4340-type steels						
3. Auger electron spectroscopy						
4. one-step temper embrittlement						
5. $500^{o}F$ embrittlement						
6. hydrogen-induced cracking						
7. hydrogen-assisted cracking						
8. ultra high strength steels						
9. impurity segregation						

ACCESSION for

NTIS

DDC

UNANNOUNCED

JUSTIFICATION

BY

DISTRIBUTION/AVAILABILITY CODES

Dist.

A

Intergranular Fracture in 4340-Type Steels:

Effects of Impurities and Hydrogen

S. K. Banerji,[*⊚] C. J. McMahon, Jr.,[*] and H. C. Feng[*†]

ABSTRACT

A study has been made of the conditions which lead to intergranular brittle fracture in 4340-type steels at an ultra high yield strength level (200 ksi, 1380 MPa) in both an ambient environment and gaseous hydrogen. By means of Charpy impact tests on commercial and high purity steels, and by Auger electron spectroscopy of fracture surfaces, it is shown that one-step temper embrittlement (OSTE or "500°F embrittlement"), and low K intergranular cracking in gaseous hydrogen are the result of segregation of P to prior austenite grain boundaries. Segregation of N also contributes to OSTE. Most, if not all, segregation apparently occurs during austenitization, rather than during tempering. Elimination of impurity effects by use of a high purity NiCrMoC steel results in an increase in K_{th} for hydrogen-induced cracking by about a factor of five (to the range 130-140 Mnm$^{-3/2}$). These observations are discussed in terms of our understanding of the mechanisms of OSTE and hydrogen-assisted cracking.

---

[*]Department of Metallurgy and Materials Science and LRSM, University of Pennsylvania, Philadelphia, PA 19104

[⊚]Now at Foote Mineral Company, Exton, PA 19341

[†]Deceased January 6, 1977

Introduction:

Ultra-high strength steels (yield strength $\geq$ 200 ksi, 1380 MPa) based on a tempered martensitic microstructure are known to be susceptible to intergranular embrittlement when tempered in the range 200 - 400°C. This has been traditionally called "350°C" or "500°F" embrittlement or, more recently, one-step temper embrittlement (OSTE)*. It is usually characterized by a trough in the plot of Charpy V-notch fracture energy as a function of tempering temperature; this is anomolous because the hardness decreases monotonically in this temperature range. The ductile-brittle transition temperature goes through a maximum corresponding to the minimum in the Charpy toughness[1]. The embrittlement is accompanied by a change in fracture mode from mainly transgranular cleavage or microvoid coalescence to predominantly intergranular separation along prior austenite grain boundaries[2]. The onset of the embrittlement coincides with the formation of cementite at the expense of ε-carbide[3,4], and it was initially believed that the precipitation of thin platelets of cementite along the grain boundaries was responsible for the embrittlement[2,3,4]. However, Capus and Mayer[5] showed that residual impurities in the steel were also an essential factor: the embrittlement was absent in a laboratory-made high purity steel of the same nominal composition as a susceptible commercial steel. The precipitation sequence of carbides in the matrix and grain boundaries of the high-purity alloy remained unchanged[5]; hence, the carbides could not be

---

*The one step is the tempering treatment, rather than tempering plus ageing at a lower temperature as in classical (two-step) temper embrittlement.

solely responsible for the loss in toughness.

The details of the interaction between impurities and carbides are not yet understood. It appears that carbides are necessary, but not sufficient, for the embrittlement. Some impurities (e.g., phosphorus) segregate to the grain boundaries in the austenite phase[6]; some rapidly diffusing species such as N could segregate to the boundaries during the subsequent tempering[7]. A carbide-rejection process could also cause an increase in impurity concentration at carbide-matrix interfaces[8,9]. In any case, localized concentrations of impurities at carbide-matrix interfaces have been shown to produce interface cracking during low temperature deformation of model alloys[9].

Ultra-high strength tempered martensitic steels have been found to be highly susceptible to intergranular crack growth in various media (e.g., H_2O, H_2, H_2S), with threshold stress intensities as low as (10-20 ksi$\sqrt{\text{in}}$)(11 - 22 MNm$^{-3/2}$). However, this problem has never been approached from the viewpoint of impurity segregation to grain boundaries, which is known to cause severe intergranular cracking of high strength steels at low stress intensities in acidic aqueous solutions[10,11].

This study was undertaken to elucidate the mechanism of intergranular embrittlement in 4340-type ultra-high strength steels. Fracture behavior in air and crack growth in a hydrogen environment were examined in a number of commercial and laboratory heats. The operative impurities in three commercially-produced 4340 steels have been identified, and the effects of these impurities on the cracking behavior of such steels in a

gaseous hydrogen environment has been determined.

Experimental Procedure:

Materials. The compositions of the steels used in this study are given in Table I. Four of the heats are commercial AISI 4340 steel, two of which (B1 and B4) were vacuum-arc-re-melted (VAR); the other two (B2 and B3) were air-melted, but one (B2) was vacuum-degassed. Heat B5 is a VAR silicon-modified 4340-type steel (300M). Heats B6 and B7 were prepared by vacuum-induction-melting from high purity materials[*], heat B6 being es-sentially a high-purity 4340 steel, and heat B7 a high-purity NiCrMo base for 4340 steel with 0.4 C. The Mn and Si were omitted from heat B7.

Heat Treatment. Austenitization was carried out in vacuum for 1 h and was followed by an oil quench. Three austenitizing temperatures were used to provide the range of grain sizes shown in Table II. Tempering treatments, usually for 1 h, were carried out in vacuum in the range 50 to $625^{o}C$.

Mechanical Testing. The toughness of each heat with various grain sizes was characterized by the fracture energy in a room temperature Charpy V-notched (CVN) test on specimens tempered at various temperatures. The degree of OSTE was indicated by the magnitude of the trough in the curve of fracture energy vs. tempering temperature.

---

[*] The base was Glidden A104 electrolytic iron.

Studies of crack growth in hydrogen gas were carried out on precracked, bolt-loaded modified WOL specimens similar to those used by Novak and Rolfe[12]. The specimen thickness was one-half inch. Shallow semicircular side-grooves with a depth equal to five percent of the specimen thickness were employed to restrict crack growth to the desired plane. The load was measured by a bolt-and-tup arrangement, with strain gauges mounted on the side faces of the tup. Pre-cracking involved electric discharge machining of a vee-slot and then generation of a fatigue crack by cyclic loading.

The compliance of specimens from each heat was determined as a function of crack length in calibration experiments. During an actual experiment, the growth of a crack at fixed displacement resulted in a decrease in the stress intensity K. Both the K value and the crack length (a) could be determined by measurement of the load, in conjunction with the compliance calibration curve, through the equation[12]:

$$K = \frac{P\ C_3\ (a/W)}{B(a)^{\frac{1}{2}}} \qquad (1)$$

where: P is applied load

a is crack length

W is specimen width

B is specimen thickness

For the present side-grooved specimens, B is replaced by $(B \times B_n)^{\frac{1}{2}}$, where B_n is the net specimen thickness. The constant C_3 (a/W) is given by[12] $\{30.96\ (a/W) - 195.8\ (a/W)^2 + 730.6\ (a/W)^3 - 1186.3 (a/W)^4 + 754.6\ (a/W)^5\}$.

Testing was carried out in a stainless steel chamber evacuated to a pressure of 10^{-3} torr and then filled with gaseous H_2 (dried by passing through a liquid nitrogen cold trap) to the desired pressure[*]. A mechanical feed-through allowed loading of the specimen after the hydrogen environment had been admitted to the test chamber.

Fracture Surface Analysis. Fracture surfaces of Charpy specimens were analysed by scanning electron microscopy (SEM) to determine the mode of fracture, with particular emphasis on the amount of intergranular fracture. Specimens given identical heat treatments to the Charpy specimens were fractured in $<10^{-10}$ torr vacuum at $\sim -100^{\circ}C$, and the fracture surfaces were analysed by Auger electron spectroscopy (AES). The percent intergranular fracture on the Auger specimens was later determined by SEM.

Results:

Fracture Behavior in Air

Commercial 4340 Steels. All four heats had essentially the same hardness, both after quenching from $850^{\circ}C$ and after tempering, as indicated by Fig. 1. The prior austenite grain size (or austenitizing temperature) had no observable effect on these

---

[*] Preliminary experiments employing a starting vacuum of 10^{-6} torr indicated no difference in crack growth behavior for the H_2 pressures used (> 1 atm).

hardness values; an example is given in Fig. 2. As shown in Fig. 3, all four 4340 heats exhibited the OSTE fracture energy trough, with the minimum occuring around 325 to 350°C. The depth of the energy trough was nearly the same in B1, B2, and B4, but the air-melted heat B3 clearly had a deeper trough than the others. The "aircraft quality" B1 steel had the highest toughness at all tempering temperatures.

The effect of prior austenite grain size on OSTE in steel B2 is shown in Fig. 4. The following aspects should be noted: First, toughness is reduced at all tempering temperatures as the grain size increases. Secondly, in the medium grain size specimens the onset of embrittlement appears to occur at a slightly lower temperature, and the minimum in the energy curve is shifted to a somewhat higher temperature than in either the fine or coarse-grained specimens. Thirdly, the depth of the energy trough is greatest for the medium grain size material. These observations may reflect the combined effects of the austenitization temperature *per se* and the austenitic grain size, as will be discussed later.

Figure 5 shows fracture surfaces of coarse grained Charpy specimens of steel B1 tempered at temperatures below, in, and above the fracture energy trough. Note that the specimen having the minimum fracture energy exhibited mostly intergranular fracture. (When the prior austenite grain size was fine (850°C austenitization), only isolated in ergranular facets could be detected in Charpy specimens having a minimum fracture energy.) Figure 6 shows that the fracture mode actually begins to change

to intergranular at tempering temperatures below 200°C, but the maximum amount of intergranular fracture corresponds to the minimum in the energy trough.

Specimens from heats B1 and B2 were broken at ~-100°C in UHV and analysed by AES. The amounts of elements found to be in excess on the (mostly) intergranular fractures were not large. Figure 7 shows the Auger spectra for steels B1 in the as-received, as-quenched, and as-tempered conditions. Figure 8 gives similar spectra from steel B2 and includes a spectrum obtained after ion sputtering. The fracture of the as-received specimens was completely transgranular cleavage; hence, these Auger data should represent the bulk composition. The as-quenched and as-tempered samples exhibited predominantly inter-granular fracture. From a detailed study of these spectra the following observations could be made for steel B1 and B2:

i) A small amount of P segregation was definitely de-tected for both B1 and B2 in both the as-quenched and tempered conditions. Because of the very small peak heights and the overlapping Mo peaks, it is not possible to be quantitative about the concentrations. However, the intergranular P concentration does not appear to be any larger after tempering than it was after austenitizing.

ii) In steel B2 (Fig. 8), there was clear evidence of N segregation to the grain boundaries in both the as-quenched and tempered conditions. Again, the concen-tration was small, and it does not appear to have in-

creased during tempering. The N peak disappeared
during ion sputtering (lowest spectrum, Fig. 8),
thus confirming that segregation had occurred at
the grain boundaries. (Note from Table I that the
air-melted steel B2 has about 3 times more free N
than the VAR steel B1.

iii) In both B1 and B2 there was a significant excess
carbon concentration at the grain boundaries in
the as-quenched condition which remained unchanged
by subsequent tempering. During ion-sputtering the
carbon peak height dropped to its bulk value (as
measured in the as-received condition). It is not
possible to tell whether this carbon was segregated
in solid solution or was associated with very fine
carbides formed by autotempering during quenching[13]
or by inadvertent tempering during the bake-out pro-
cess of the Auger vacuum system: however, the peak
shape looks more like elemental C than carbide.

A similar analysis on a coarse grain specimen of steel B3
(air-melted) tempered at $350^{o}C$ showed clear evidence of P, N,
and C in excess on an intergranular fracture surface.

High-Purity 4340-Type Steels. In order to determine the
magnitude of the impurity effects in OSTE, experiments were
carried out on high-purity laboratory heats B6 and B7. Table III
shows that the 0.2% offset yield stress and the ultimate tensile
strength of these steels were essentially the same as the com-

mercial 4340 steels (following a 850°C quench and 350°C temper).
The hardness values were also nearly identical to those of the
commercial steels, as shown in Fig. 9. However, the energy
trough indicative of OSTE was absent in the NiCrMo pure base
steel (heat B7), as shown in Fig. 10. Here the fracture energy
increased gradually up to about 350°C, then very rapidly at
higher temperatures as softening of the steel continued. Note
the difference in energy scales in Figs. 3 and 10 and the com-
parison between the pure heat B7 and the best of the 4340 steels,
B1.

Figure 11 shows the effect of austenitizing temperature in
steel B7. Although the general level of the fracture energy
curve was reduced as the prior austenite grain size was increased,
the OSTE energy trough was absent in even the coarse grain condi-
tion. The coarse grain specimen fractured at 350°C exhibited
essentially no intergranular fracture; an example is shown in Fig.
12 (compare with Fig. 5). The absence of both the OSTE energy
trough and the intergranular mode of fracture are attributed
only to the lack of impurities in this pure steel, since the car-
bide precipitation mechanism or sequence should not be altered
by the purity of the steel[5].

When the typical commercial levels of Mn and Si were added
to the NiCrMo pure base alloy to make a "pure" 4340 steel (heat
B6), the Charpy results were similar to those of the commercial
steels. This is illustrated in Fig. 13, which compares the
fracture energies of heats B6 and B1. The energy trough re-
appeared with the addition of Si and Mn, although the toughness

of B6 was somewhat higher than for B1 at all tempering temperatures, as would be expected in a VIM steel. The fracture mode was partly intergranular and partly a mixture of cleavage and rupture, as shown in Fig. 14.

Silicon-Modified (300M) Steel. Silicon additions are known to retard the kinetics of tempering of 4340 steel by stabilizing ϵ-carbide and inhibiting the formation of cementite[14,15]. Thus, a Si-modified 4340-type steel retains a high hardness to higher tempering temperatures, as shown in Fig. 1. The effect of Si on the Charpy fracture energy is shown in Fig. 15. The OSTE energy trough in the 300M heat (B5) was spread out over a wider range of temperature (250-450$^{\rm o}$C), with the minimum at about 450$^{\rm o}$C. However, the depth of the energy trough was about the same as in 4340. When the prior austenite grain size of the 300M steel was increased, the entire Charpy energy curve was shifted downward, as expected; the energy trough was even more spread out ($\approx$250-525$^{\rm o}$C), with the minimum at $\approx$525$^{\rm o}$C. This is shown in Fig. 16, which also indicates that no intergranular fracture occurred until a tempering temperature of $\approx$375$^{\rm o}$C. Above that, the incidence of intergranular fracture increased sharply, with a peak occurring at $\approx$525$^{\rm o}$C, corresponding to the minimum in the energy curve. Figure 17 shows the fracture mode for the Charpy specimen tempered at 525$^{\rm o}$C; it was almost completely intergranular.

Hydrogen-Assisted Cracking

Crack growth in bolt-loaded WOL specimens was monitored

by recording the drop in load on the tup (load cell). In the
early experiments the analog (mv) signal was displayed directly
on a strip chart recorder, but in most cases an analog-to-digital
converter was used and the reading was recorded on punch-tape
and teletype. In the early (rapid) stages of crack growth, read-
ings were taken every three seconds; the time interval was in-
creased as the crack slowed down. Load readings were converted
to crack length a and stress intensity K values by computer via
an equation fitted to the compliance curve.

In general, crack lengths were found to vary smoothly with
time, in contrast with the discontinuous, stepwise growth ob-
served by Briant et al.[16] in a lower strength (HY130) steel.
Examples of a vs t curves are given in Fig. 18a, which shows a
threshold determination in steel B2, and Fig. 18b, which shows
the smoothness of the curve for a B7 specimen on an expanded
time scale. Crack growth rates were determined by simply taking
the slopes of the (essentially) lienar segments of the a vs t
curves, as shown in Fig. 18. In this way, conventional[17,18] plots
of log v (= log $\frac{da}{dt}$) vs K were obtained in the form of segmented curves,
as shown in Fig. 19. In a number of cases, the crack did not
come to rest within the range a/W $\leq$ 0.8, which is the limit of
validity of the compliance curve; hence, threshold values of
stress intensity K_{th} could not always be determined.

In an effort to determine the effect of tempering temper-
ature in a commercial steel, log v vs K curves were obtained
for fine grain specimens of heat B1 tempered between 200°C and

400°C, as shown in Fig. 19. Contrary to expectations prompted by the Charpy data (e.g., Fig. 3), no significant differences could be found in these specimens. All had K_{th} values <20 MNm$^{-3/2}$ and the stage II values of v were more-or-less equivalent. In all cases, the fracture mode was entirely intergranular; an example is given in Fig. 20. Thus, it is clear that steel B1 is highly susceptible to hydrogen-assisted cracking at low K levels, regardless of the degree of OSTE present in the steel.

Specimens of steel B2, in which both the prior austenite grain size and the tempering temperature were varied, were tested in a similar way. As shown in Fig. 21, these specimens exhibited behavior essentially similar to steel B1, and neither tempering temperature nor grain size was found to be a significant variable in this commercial steel. Again, all hydrogen-assisted fractures were intergranular. Note that in four cases duplicate specimens were tested; these data indicate the variability that can be expected in the log v vs K behavior of supposedly identical specimens.

Steels B6 and B7, having been prepared in an effort to see if impurity effects could be eliminated, were similarly tested in the fine grain condition, after tempering at 350°C. Fig. 22 shows that the K_{th} value in steel B7 is 5-to-6 times higher than in the commercial steels B1 and B2 when tested under the same conditions at the same strength level. The B7 specimen with $K_{th} \approx 120$ MNm$^{-3/2}$ exhibited a few intergranular facets on the fracture surface, the rest being cleavage and rupture. The other B7 specimen had no intergranular fracture, as shown in Fig. 23. A test on a fine grain B7 specimen at 30 psig hydrogen (23°C) gave a K_{th} of ~100 MNm$^{-3/2}$, and the fracture

was a mixture of cleavage and intergranular.

Some log v vs K data for the B6 steel are also shown in Fig. 22, and the fracture mode is illustrated in Fig. 24. It is apparent that the addition of Mn and Si to the pure base steel caused the reappearance of the low stress, intergranular fracture. This is consistent with the simultaneous reappearance of OSTE (cf. Fig. 13).

The effect of prior austenite grain size on the hydrogen-assisted cracking behavior of steel B7 was also determined. Figure 25 indicates that a substantial reduction in K_{th} occurs when the grain size is increased. This is in contrast with the behavior of the commercial 4340 steel, described earlier (cf. Fig. 21).

Finally, a test on a 300M steel (B5) specimen indicated the same low K_{th}, intergranular fracture behavior observed in the other commercial steels, as shown in Fig. 26.

Discussion

One-Step Temper Embrittlement. The anomolous fracture energy trough associated with OSTE has been shown to be an impurity effect. As in the previous study by Capus and Mayer[5], this can be demonstrated in an indirect way by the absence of the energy trough in a high purity NiCrMoC steel (B7). In the present study, direct evidence by AES of the segregation of P (and of N in an air melted steel) to prior austenite grain boundaries has been obtained.

It appears that much, if not all, of the segregation of P and N occurred in the γ-phase, since the concentrations did not increase as a result of tempering. It is to be expected that the segregation of P would be severely limited in the temperature range where OSTE is observed. This can be seen from Figure 27 which gives the characteristic diffusion distances of P and N in a 1 h tempering treatment at various temperatures. It can be seen that some N segregation to grain boundaries could occur in the temperature of interest; however, the limited amount of Auger data available indicate that this does not occur, presumably because N segregates to dislocations, instead, in a tempered martensite microstructure.

We have seen that the addition of Mn and Si to the high purity steel caused the reappearance of OSTE. Rather than an effect of either Mn or Si *per se*, we suggest that this effect is the result of promotion of segregation of P in austenite by Mn, and perhaps Si, even though this steel contains only 0.003% P. This suggestion is based on the demonstration of Kaneko et al.[19] of the strong interaction of Mn and Si with P in the austenite phase, as shown in Figure 28. It is also supported by recent results obtained by Clayton[20], who found an enhancement of P segregation in austenite in a NiCr steel when the Mn concentration was increased.

If the P or N concentration in prior austenite grain boundaries does not increase during a tempering treatment, then the susceptibility to OSTE from P or N is inherited from the austenitization treatment. The rejection of these impurities by car-

bides formed in grain boundaries during tempering would not be the operative embrittlement mechanism, as suggested earlier[8,9]. However, since the onset of the embrittlement phenomenon is co-incident with the precipitation of cementite, one must ask what is the role of the carbides. We suggest that it is as follows: Brittle fracture in the temperature region of the Charpy energy trough is initiated by intergranular cracks at the tip of blocked slip bands, i.e., dislocation pile-ups. Grain boundary carbide platelets behave elastically in this temperature range and would therefore act as effective barriers to dislocations. Without such platelets, dislocation pile-ups may be relieved by slip in neighboring grains.

Hydrogen-Assisted Cracking. Experiments on 4340 and 300M steels have shown that these commercial steels are highly sus-ceptible to intergranular hydrogen-assisted cracking at low K_{th} (less than 30 MN/m^2). The susceptibility is not affected signi-ficantly by the degree of OSTE present or by the austenite grain size. However, this effect is absent in the high purity NiCrMoC steel; here, the hydrogen-induced fracture mode is transgranular (cleavage and rupture), and K_{th} is raised by at least a factor of five. Hence, we conclude that this high K_{th}, transgranular fracture behavior represents the intrinsic effect of hydrogen in such a steel; the low K_{th}, intergranular fracture is shown to be an impurity effect. As observed in the OSTE phenomenon, the addition of Mn and Si caused a return of the "hydrogen em-brittlement", presumably because of their effect on the segre-gation of residual P in this steel.

It appears that for the development of commercial steels with high resistance to OSTE and hydrogen induced cracking one must eliminate intergranular segregation of P, and perhaps other impurities, during austenitization. To do this several steps may be tried:

1. Reduce the concentration of alloying elements that promote P segregation in austenite, such as Cr, Mn and Si.

2. Use elements which scavenge P, such as Mo and Ti, and an element which scavenges N, such as Al.

3. Increase the Ni concentration to promote toughness; this may be permissible since Ni interacts weakly with P[19].

In view of the very small concentrations of P detected in the prior austenite grain boundaries of the present steels, one might wonder why such a large effect is observed. The answer lies in the very large amplification of impurity effects which can be exerted by the high hardness (or yield strength) level in these ultra-high strength steels. This can be demonstrated by extrapolation of the data of Mulford et al..[21] as shown in Figure 29. Here it can be seen that low P concentrations which would be virtually innocuous at low hardness levels could be quite damaging as the hardness level is increased. This can be understood in terms of the effect of yield stress on the local stress concentration at the tip of a dislocation pile-up. As discussed in detail elsewhere[22], the nucleation of a brittle crack requires that the sum of the continuum stress concentration and the dislocation stress concentration equal the local cohesive strength of the steel. This can be expressed as:

$$\sigma_{COH}(H, i) = n\sigma_Y + \frac{2L}{Gb}\left(\frac{\sigma_Y}{\sqrt{3}} - \tau_f\right)^2$$

where $\sigma_{COH}(H,i)$ is the intergranular cohesive strength and is
a function of the local hydrogen and impurity concentration; n
is a factor in the range one-to-three, found by methods of con-
tinuum mechanics; σ_Y is the tensile yield stress; τ_f is the dislocation friction
stress, and L is the length of a dislocation pile-up. It can be seen that
the concentrated stress increases with (yield strength)^2. Thus, the required
amount of reduction in σ_{COH} due to hydrogen or impurities for
brittle crack nucleation must decrease as the yield strength
increases.

We have seen that even in the high purity steel (B7), some
variability exists in the resistance to hydrogen-induced cracking.
One specimen exhibited a small amount of intergranular fracture
and a K_{th} about 20 $MNm^{-3/2}$ less than the other, even though this
steel contained only about 0.003% P. This behavior is presumably
the result of an inhomogeneous distribution of that small amount
of P in this steel.

Effect of Austenitizing Temperature. An increase in austenitizing temper-
ature produces not only an increase in the austenite grain size, but also a
small decrease in the amount of segregated P, as shown by the work of Ogura
et al.[23] on a NiCr steel. The general lowering of the Charpy
fracture energy curve with increasing austenitizing temperature
is presumably the result of the increase in prior austenite grain
size. The exaggerated depth of the fracture energy trough ob-

served for the intermediate austenitizing temperature in steel B2 (Figure 4) may simply be the result of the worst combination of simultaneously increasing the grain size and decreasing the concentration of segregated P .

In a fine grained steel the onset of OSTE is thought to coincide with the formation of isolated intergranular micro-cracks which act as nuclei for cleavage cracks. Thus, the onset of easy crack nucleation is responsible for the reduction in Charpy fracture energy. In coarse grained Charpy specimens, the intergranular microcracks are larger and more readily connected. Therefore, not only is an energy trough produced, but the whole energy curve is shifted downward. In the high purity steel (B7), also. the fracture energy curve is shifted downward as the grain size is increased. However, here intergranular fracture is not an issue; the increase in toughness with decreasing grain size is presumably due to micro-structural refinement (e.g., of martensite lath colonies).

In commercial steels, the austenite grain size has no apparent effect on the K_{th} value, but grain size exerts a large effect in the high purity steel. Presumably, the commercial steel has so much segregated P that even grain refinement can not improve it. However, as steels with less P segregation are developed, austenite grain refinement should become an important means of providing increased resistance to hydrogen-assisted cracking.

The present results indicate that the use of high temperature austenitizing treatments should be explicitly discouraged. Although high temperature austenitizing can lead to an increase

in sharp-crack fracture toughness K_{Ic}[24], this is apparently an artifact of the sharp-crack test which is observed when the plastic zone size at the crack tip is less than the prior austenite grain size[25]. This anomoly is absent in a blunt notch test with its larger plastic zone size.

Conclusions

1. The trough in Charpy fracture energy and concomitant intergranular fracture, indicative of OSTE, which occurs in commercial 4340-type steels is shown to be absent in a high purity NiCrMoC steel of the same microstructure and strength. This indicates indirectly that OSTE is an impurity effect.

2. This conclusion has been confirmed directly by AES studies of prior austenite grain boundaries of commercial steels fractured in UHV in which P was found to be segregated to prior austenite grain boundaries in a vacuum-arc-remelted steel; both P and N were found segregated in air melted steels.

3. In appears that the intergranular P and N concentrations do not increase during tempering, indicating that the segregation is inherited from the austenitizing treatment.

4. An addition of Mn and Si to the high purity steel caused a return of OSTE; this is interpreted as being due to the promotion of P segregation in austenite by Mn, and perhaps Si. This interpretation is shown to be consistent with related observations in other laboratories.

5. Stable crack growth in a gaseous hydrogen atmosphere

occurs much more smoothly and continuously in 4340-type
steels at ultra-high strength levels than in a lower
strength (HY130) steel.

6. All of the commercial steels examined were quite suscep-
tible to low K_{th}, intergranular cracking in hydrogen, regard-
less of heat treatment or prior austenite grain size.

7. The high purity NiCrMoC steel had a K_{th} level higher by
a factor of five-to-six than the commercial steels, and
the mode of cracking was transgranular (rupture and
cleavage) at the highest K_{th} level.

8. The K_{th} of this high purity steel was reduced by an increase
in the prior austenite grain size, in contrast with the be-
havior in commercial steels.

9. The addition of Mn and Si to this high purity steel, which
caused the return of OSTE, also caused the low K_{th}, intergran-
ular cracking to reappear.

10. These results indicated that the resistance to hydrogen embrit-
tlement in ultra-high strength 4340-type steel can be greatly
improved if impurity effects are brought under control.

ACKNOWLEDGEMENTS

References

1. R. L. Rickett and J. M. Hodge; Proc. ASTM, 1951, Vol. 51, p. 931.

2. M. A. Grossman; Trans. AIME, 1946, Vol. 167, p. 39.

3. L. J. Klinger, W. J. Barnett, R. P. Frohmberg, and A. R. Troiano; Trans. ASM, 1954, Vol. 46, p. 1557.

4. B. S. Lement, B. L. Averbach, and M. Cohen; Trans. ASM, 1954, Vol. 46, p. 851.

5. J. M. Capus and G. Mayer; Metallurgia, 1960, Vol. 62, p. 133; J. Iron Steel Inst., 1958, Vol. 196, p. 255; ibid, 1963, Vol. 201, p. 53.

6. B. J. Schulz and C. J. McMahon, Jr.; in "Temper Embrittlement of Alloy Steels", ASTM STP 499, 1972, p. 104.

7. C. J. McMahon, Jr.; Mater. Sci. and Eng., 1976, Vol. 25, p. 233.

8. E. B. Kula and A. A. Anctil; J. of Matls. ASTM, 1969, Vol. 4, p. 817.

9. J. R. Rellick and C. J. McMahon, Jr.; Met. Trans., 1974, Vol. 5, p. 2439.

10. U. Q. Cabral, A. Hache, and A. Constant; C. R. Acad. Sci. Paris, 1965, Vol. 260, p. 6887.

11. K. Yoshino and C. J. McMahon, Jr.; Met. Trans., 1974, Vol. 5, p. 363.

12. S. R. Novak and S. T. Rolfe; J. of Matls. ASTM, 1969, Vol. 4, p. 701.

13. A. J. Baker, F. J. Lauta, and R. P. Wei: "Structure and Properties of Ultra-High Strength Steels", ASTM STP 370, 1965, p. 3.

14. A. G. Allten and P. Payson; Trans. ASM, 1953, Vol. 45, p. 498.

15. C. J. Alstetter, M. Cohen, and B. L. Averbach; Trans. ASM, 1962, Vol. 55, p. 287.

16. C. L. Briant, H. C. Feng and C. J. McMahon, Jr; submitted to Met. Trans. A.

17. H. G. Nelson and D. P. Williams: "Quantitative Observations of Hydrogen-Induced Slow Crack Growth in a Low Alloy Steel", NASA Tech. MEMO X-62, March, 1973.

18. S. J. Hudak and R. P. Wei; Met. Trans., 1976, Vol. 7A. p. 235.

19. H. Kaneko, T. Nishizawa, K. Tamaki, and A. Tanifuji; J. Japan Inst. of Metals 1965, Vol. 29, p. 166.

20. J. Q. Clayton; Ph. D. Thesis, Cambridge University, 1977.

21. R. A. Mulford, C. J. McMahon, Jr., D. P. Pope, and H. C. Feng; Met. Trans. A, 1976, Vol. 7A, p. 1183.

22. C. J. McMahon, Jr., C. L. Briant, and S. K. Banerji; to be published in the Proc. 4th Int. Conf. on Fracture, Waterloo, Canada, June (1977).

23. T. Ogura, C. J. McMahon, Jr., and H. C. Feng; to be published.

24. G. Y. Lai, W. E. Wood, R. A. Clark, V. F. Zackay, and E. R. Parker; Met. Trans., 1974, Vol. 5, p. 1633.

25. R. O. Ritchie, B. Francis, W. L. Server; Met. Trans. A, 1976, Vol. 7A, p. 831.

26. C. Wert; Phys. Rev., 1950, Vol. 79, p. 601.

27. P. W. Gruzin and V. V. Minal: Fiz. Metall. Metalloved, 1963, Vol. 16, p. 551.

Table I: Chemical Compositions (wt. %)

Heat	Steel	C	Ni	Cr	Mn	Si	Cu	Al	Mo	S	P	V	Cb	N/N*
B1	4340 VAR	0.38	1.50	0.85	0.75	0.20	0.14	0.05	0.20	0.004	0.006	-	-	6/72
B2	4340 AM**	0.39	1.72	0.73	0.68	0.08	-	0.046	0.22	0.016	0.009	0.05	0.04	18/67
B3	4340 AM	0.45	1.90	0.70	0.65	0.24	0.18	0.01	0.23	0.024	0.015	-	-	-
B4	4340 VAR	0.41	1.75	0.79	0.80	0.26	0.06	-	0.23	0.004	0.006	-	-	-
B5	300M VAR	0.42	1.76	0.76	0.76	1.59	-	-	0.41	0.002	0.007	0.10	-	-
B6	High-Purity VIM 4340	0.37	1.80	0.75	0.5(?)	0.44	-	-	0.26	0.005	0.003	-	-	.001⊥
B7	High-Purity VIM NiCrMo base	0.37	1.80 -1.84	0.77 -0.85	.007	0.002	.002	<.001	0.25	0.003	0.003	-	-	.001⊥

VAR = vacuum arc remelted
VIM = vacuum induction melted
AM = air melted
N/N* = ratio of free to compounded N in ppm (N* is compounded N)
** = Heat B2 was vacuum degassed
⊥ = Free N

Table II: Austenitizing Temperatures and Grain Sizes

Temperature (^{O}C)	ASTM No.
850	8-10
1000	6-7
1160	3-5

Table III: 0.2% Offset Yield Stress and Ultimate Tensile
Strength of Steels B1, B6, and B7 Austenitized
at 850°C; tempered 1 h at 350°C.

Steel	Yield Stress, 0.2% Offset		Tensile Strength	
	$(10^3 psi)$	(MPa)	$(10^3 psi)$	(MPa)
B1 (Commercial 4340)	201	1386	240	1655
B6 (High-Purity 4340)	196	1351	231	1593
B7 (High-Purity NiCrMo)	206	1420	226	1558

Figure Captions

1. Variation of hardness with tempering temperature in various 4340 steels and a 300M steel.

2. Variation of hardness with tempering temperature in steel B1(4340) with two different austenitizing temperatures.

3. Variation of Charpy V-notch fracture energy with tempering temperature for four heats of 4340 steel. Room temperature tests.

4. Effect of austenitizing temperature on the room temperature Charpy V-notch fracture energy as a function of tempering temperature in steel B2.

5. Fracture surfaces of Charpy specimens of steel B1 austenitized at 1160°C and tempered at (a) 250°C, (b) 400°C, and (c) 500°C.

6. Correlation of the incidence of intergranular fracture with the fracture energy trough in steel B1.

7. Auger spectra from fracture surfaces of steel B1 fractured in UHV in the as-received, as-quenched, and as-tempered conditions. The P and C peaks are circled in each case.

8. Auger spectra from fracture surfaces of steel B2 fractured in UHV in the as-received, as-quenched, as-tempered, and ion sputtered conditions. The P, C and N peaks are circled.

9. Variation of hardness with tempering temperature in steels B6 and B7 compared with steel B1.

10. Room temperature Charpy fracture energy as a function of tempering temperature for steel B7 compared with steel B1.

11. Effect of austenitization temperature on the room tempera-
ture Charpy fracture energy of the "pure" steel B7.

12. Fracture surface of Charpy specimen of steel B7 austenitized
at $1150^{o}C$ and tempered at $350^{o}C$, showing no intergranular
fracture.

13. Variation of Charpy fracture energy as a function of temper-
ing temperature for steel B6 compared with steel B1, showing
that addition of Mn and Si to the pure heat (B7) re-introduces
the fracture energy trough.

14. Fracture surface of Charpy specimen steel B6 austenitized
at $1150^{o}C$, tempered at $350^{o}C$; compare with Fig. 12.

15. Variation of Charpy fracture energy with tempering temperature
for steel B5 compared with steel B1, showing that a Si addi-
tion causes the fracture energy trough to occur at higher
temperatures and over a larger temperature range.

16. Correlation of incidence of intergranular fracture with
the fracture energy trough in steel B5.

17. Fracture surface of Charpy specimen of steel B5 austenitized
at $1160^{o}C$, tempered at $525^{o}C$.

18. Examples of variation in crack length as a function of
time in steels tested as WOL specimens in hydrogen at
$23^{o}C$, 1 psig. (a) shows curve for steel B2 on an extended
time scale for a specimen in which a crack arrest was
achieved. (b) shows a curve for steel B7 on an expanded
time scale in which the early stages of crack growth can
be seen.

19. Crack growth rate as a function of stress intensity in steel B1 tempered at various temperatures.

20. Hydrogen-induced fracture surface in WOL specimen of steel B1 austenitized at 850°C, tempered at 250°C.

21. Crack growth rate as a function of stress intensity in WOL specimens of steel B2 austenitized at various temperatures and tempered between 200 and 350°C, as indicated.

22. Crack growth rate as a function of stress intensity in steels B7 and B6 compared with that in steel B2. Duplicate specimens of all three steels were tested.

23. Fracture surface of WOL specimen of steel B7 fractured in hydrogen, showing fracture mode to be rupture and cleavage.

24. Fracture surface of WOL specimen of steel B6 fractured in hydrogen showing intergranular fracture mode.

25. Crack growth rate as a function of stress intensity in WOL specimens of steel B7 having three different prio austenite grain sizes.

26. Crack growth rate as a function of stress intensity for steel B5 (300M) compared with two specimens of steel B2 (4340).

27. Characteristic diffusion distance for a 1 h exposure at various temperatures for P and N in α-Fe.

28. Effect of alloying elements on the solubility of P in γ-Fe containing 12% Ni at 1000°C, from Kaneko et al. Ref. 19.

29. Effect of hardness on ductile-brittle transition in a NiCr steel doped with P from Mulford et al., Ref. 21, showing that extrapolation to high hardness levels would result in a large embrittling effect for a small amount of impurity.

FIG. 1

FIG. 2

FIG. 3

FIG. 4

a

b

20μ

c

FIG 5

FIG. 6

JOULES

25 30 15 10 5 0

TEMPERING TEMPERATURE, C

0   100   200   300   400   500

STEEL - B1
1160 C, 1h, OQ
TEMPERED 1h

20 15 10 5 0 100 75 50 25 0

% LG FRACTURE   CVN FRACTURE ENERGY, ft-lbs

FIG. 7

FIG.8
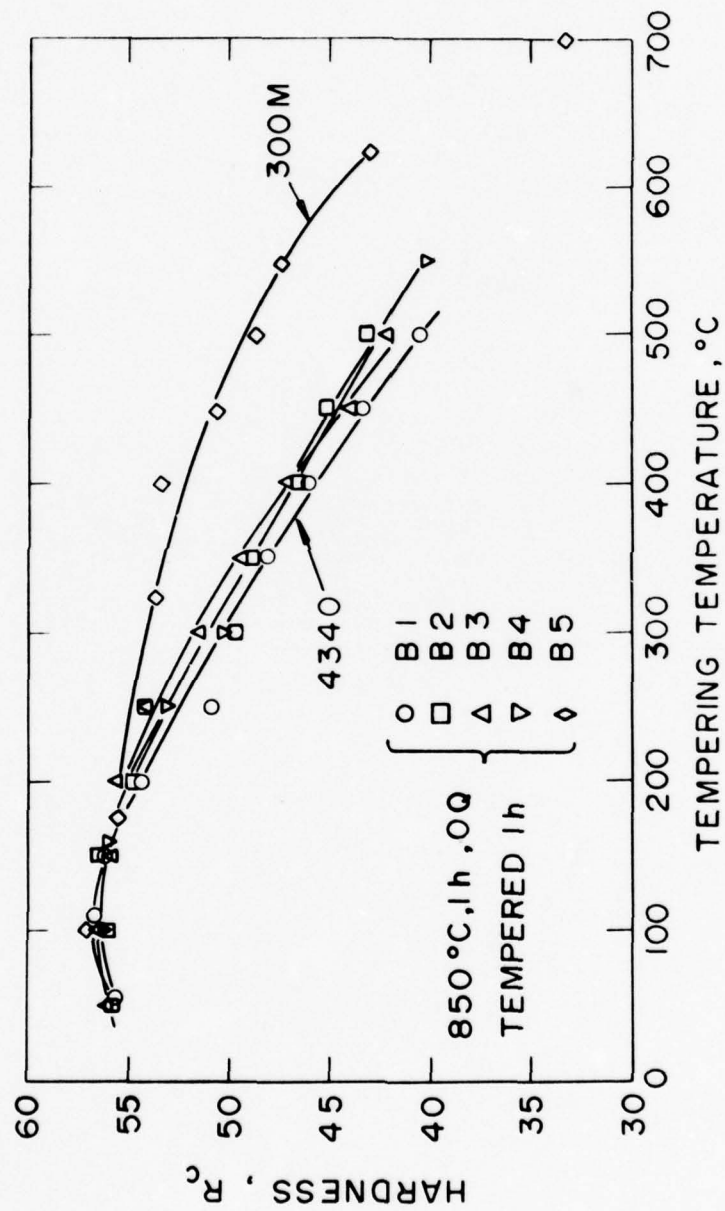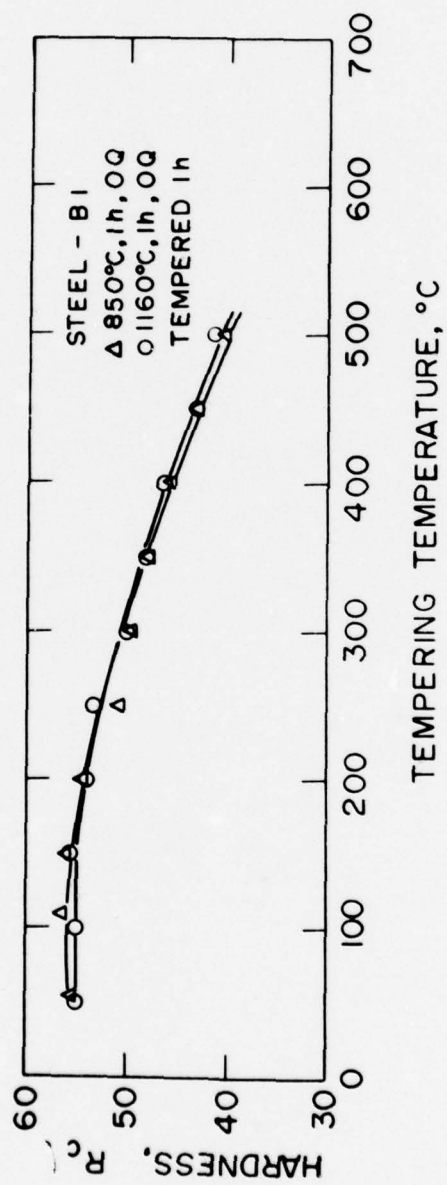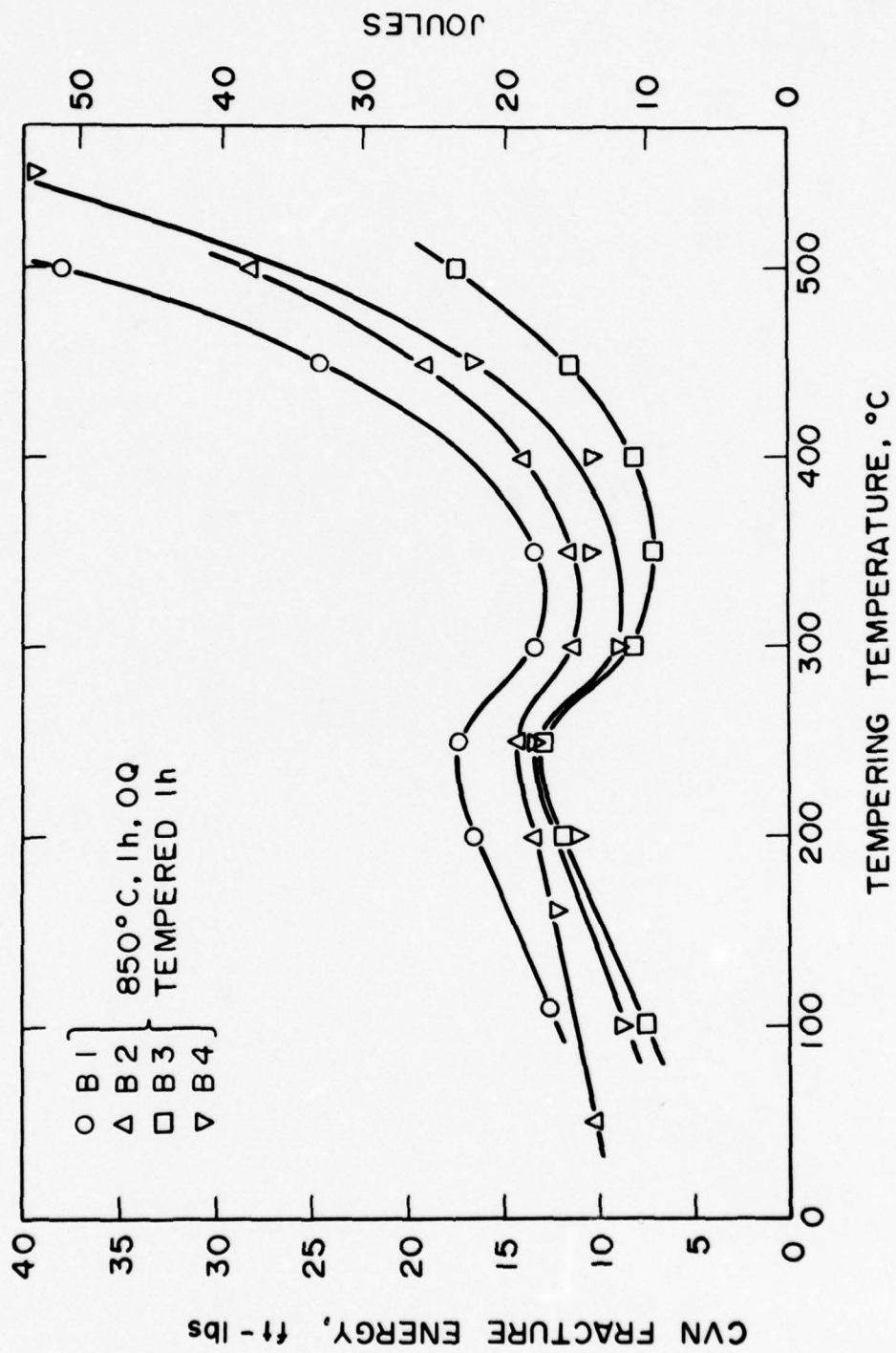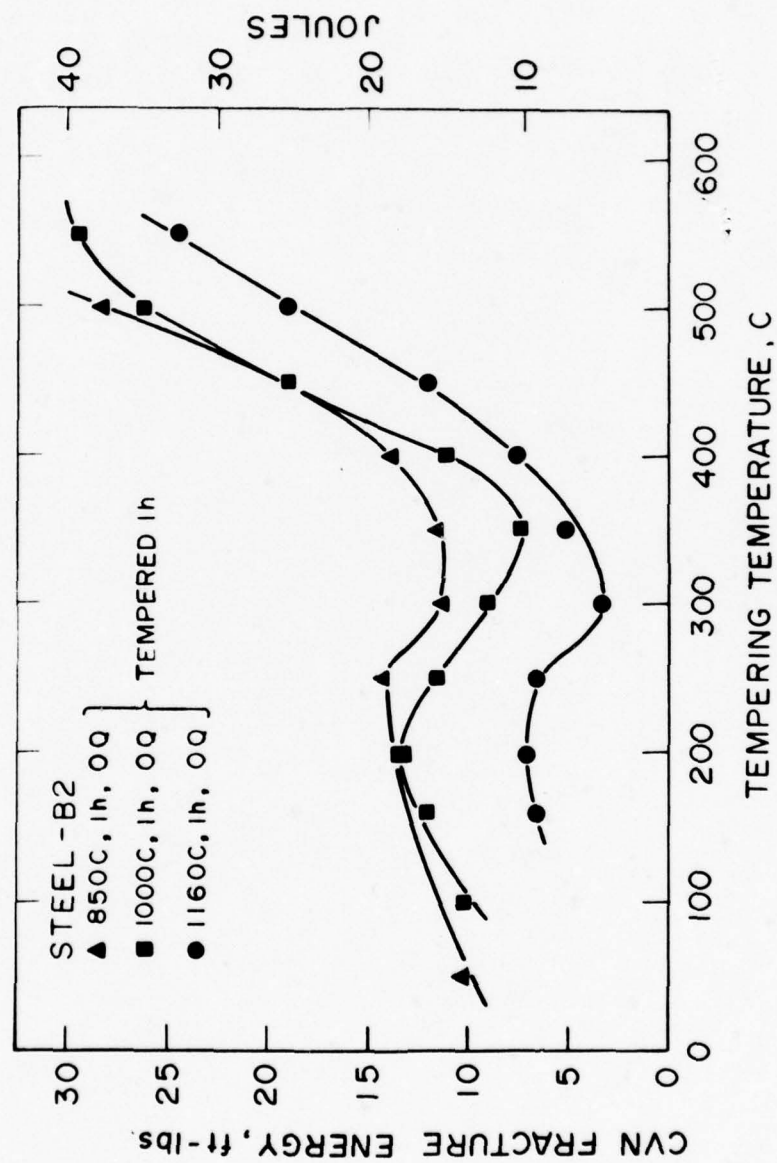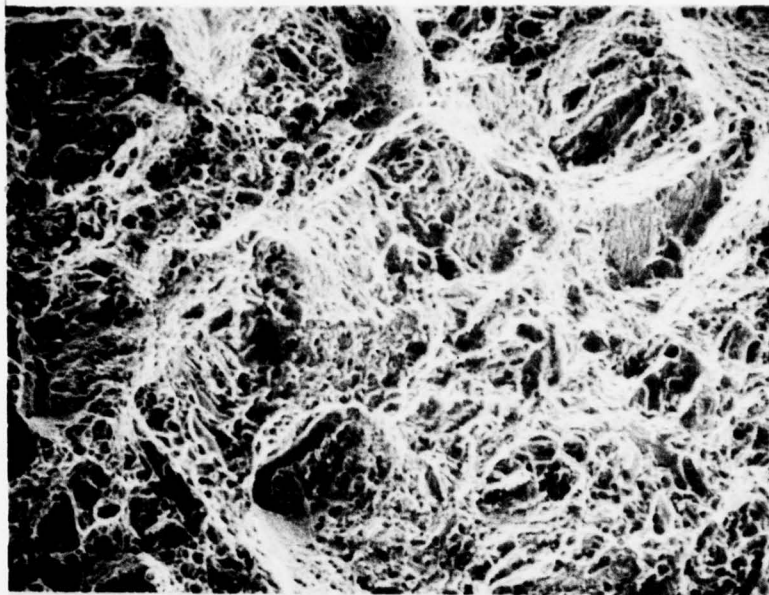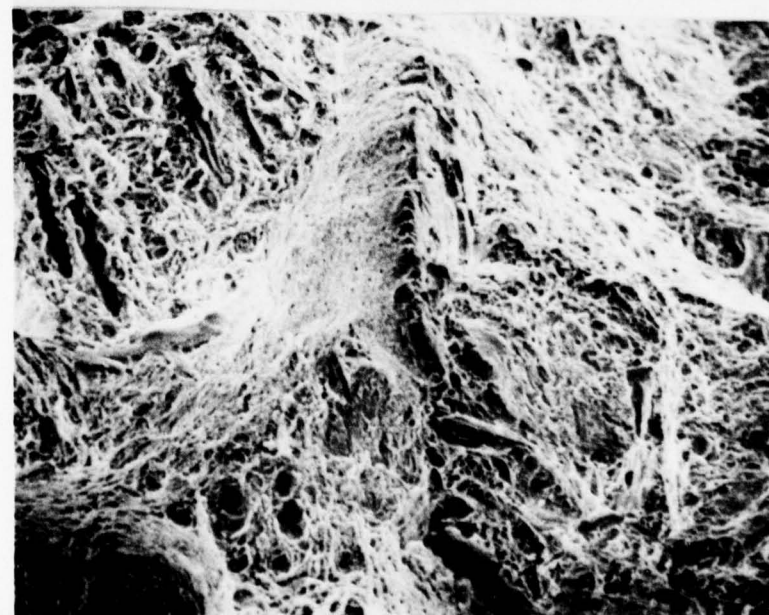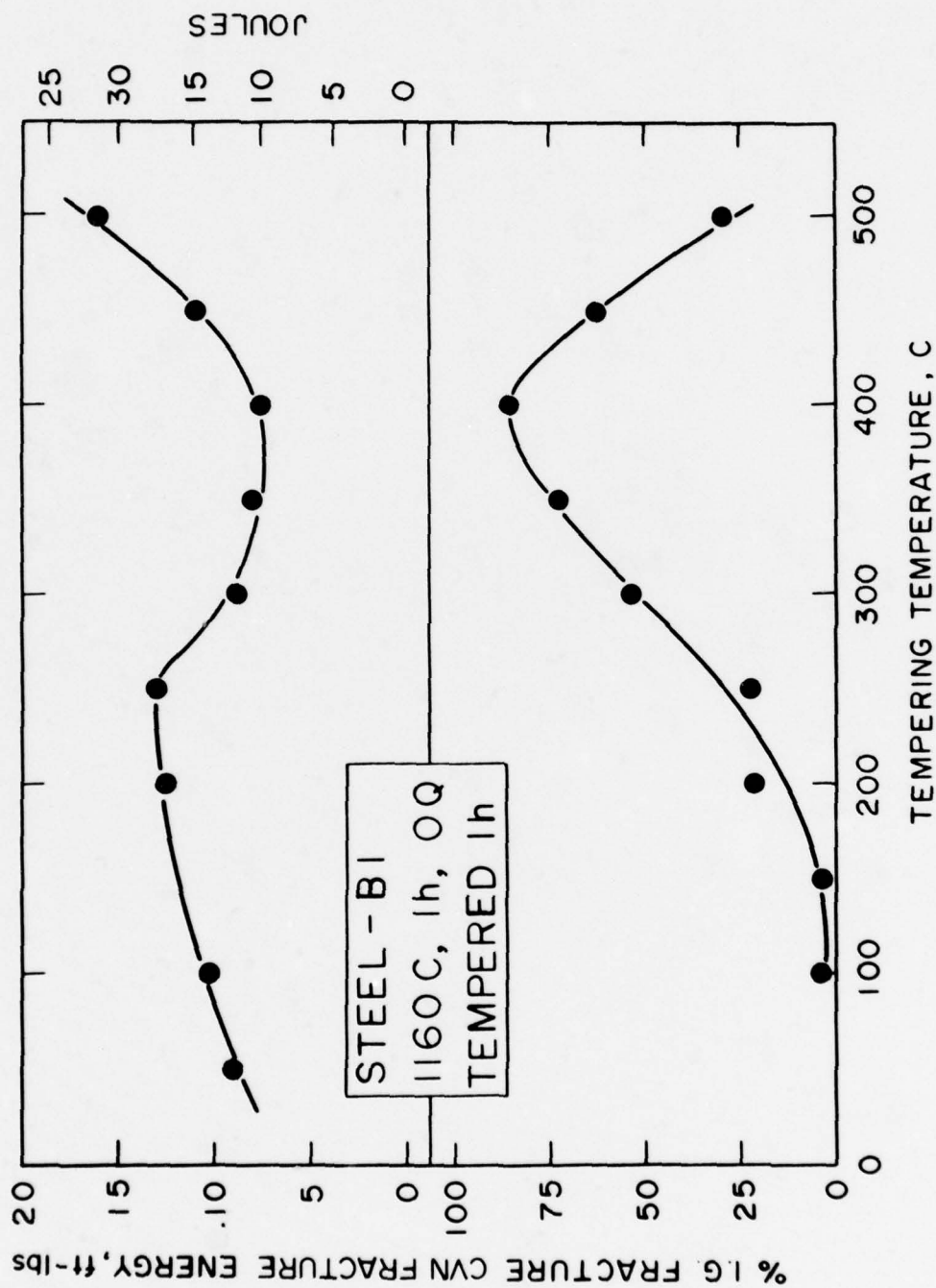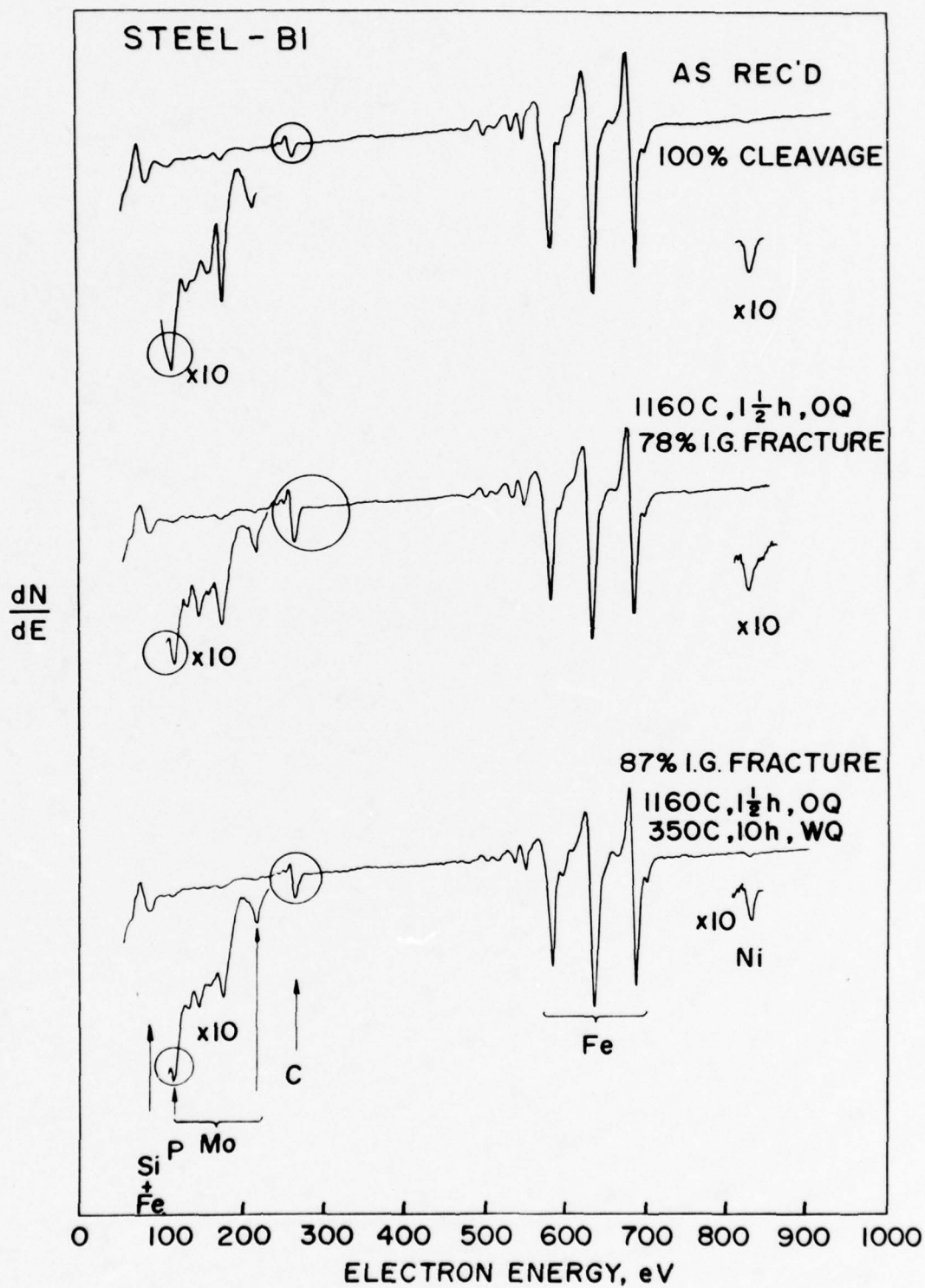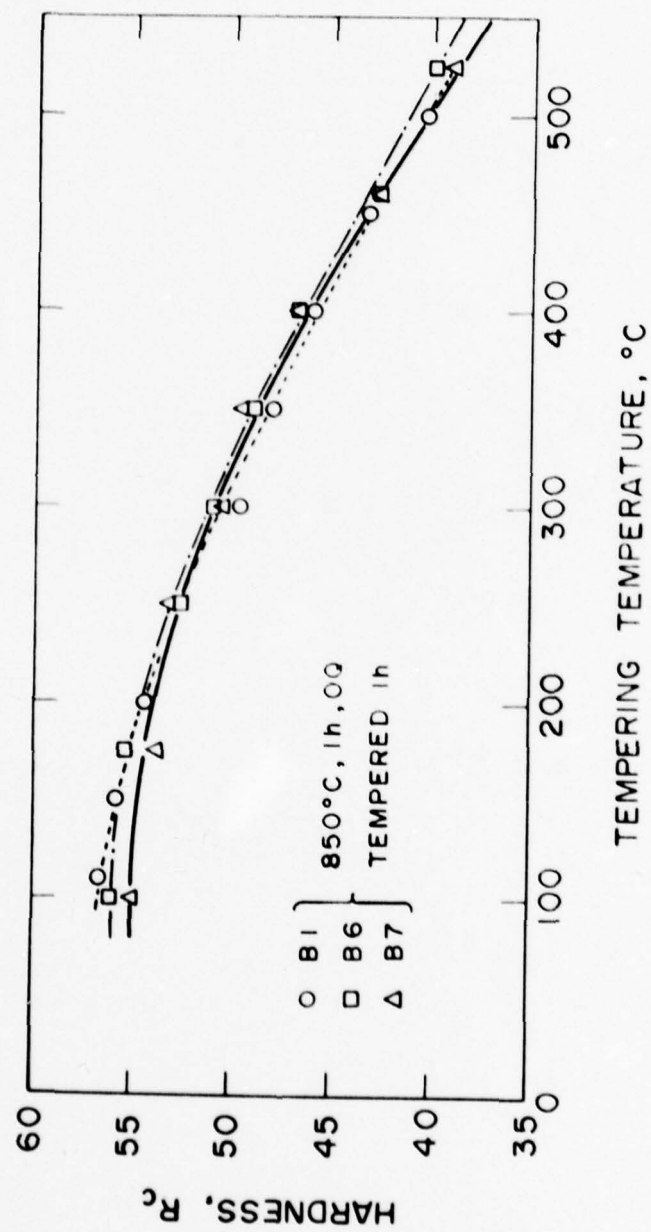
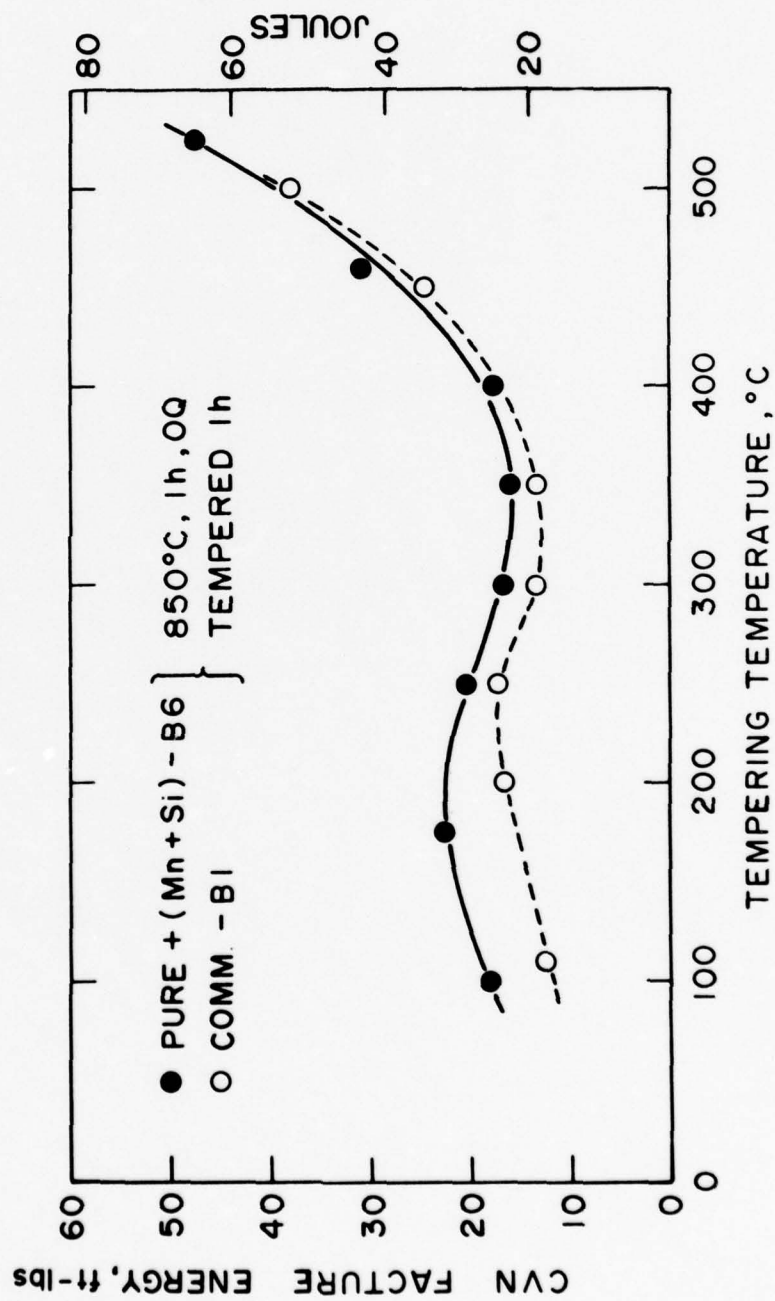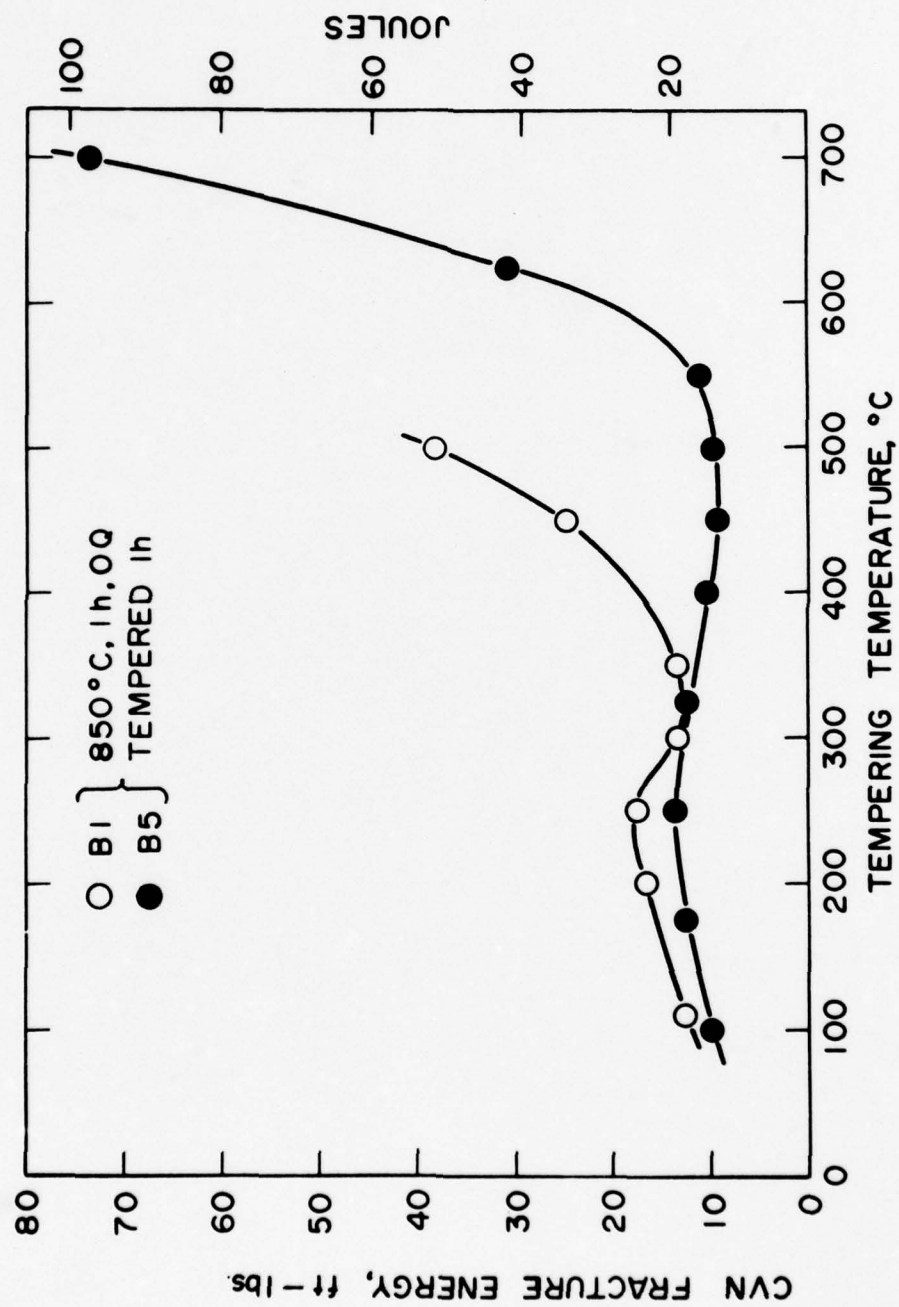FIG. 9
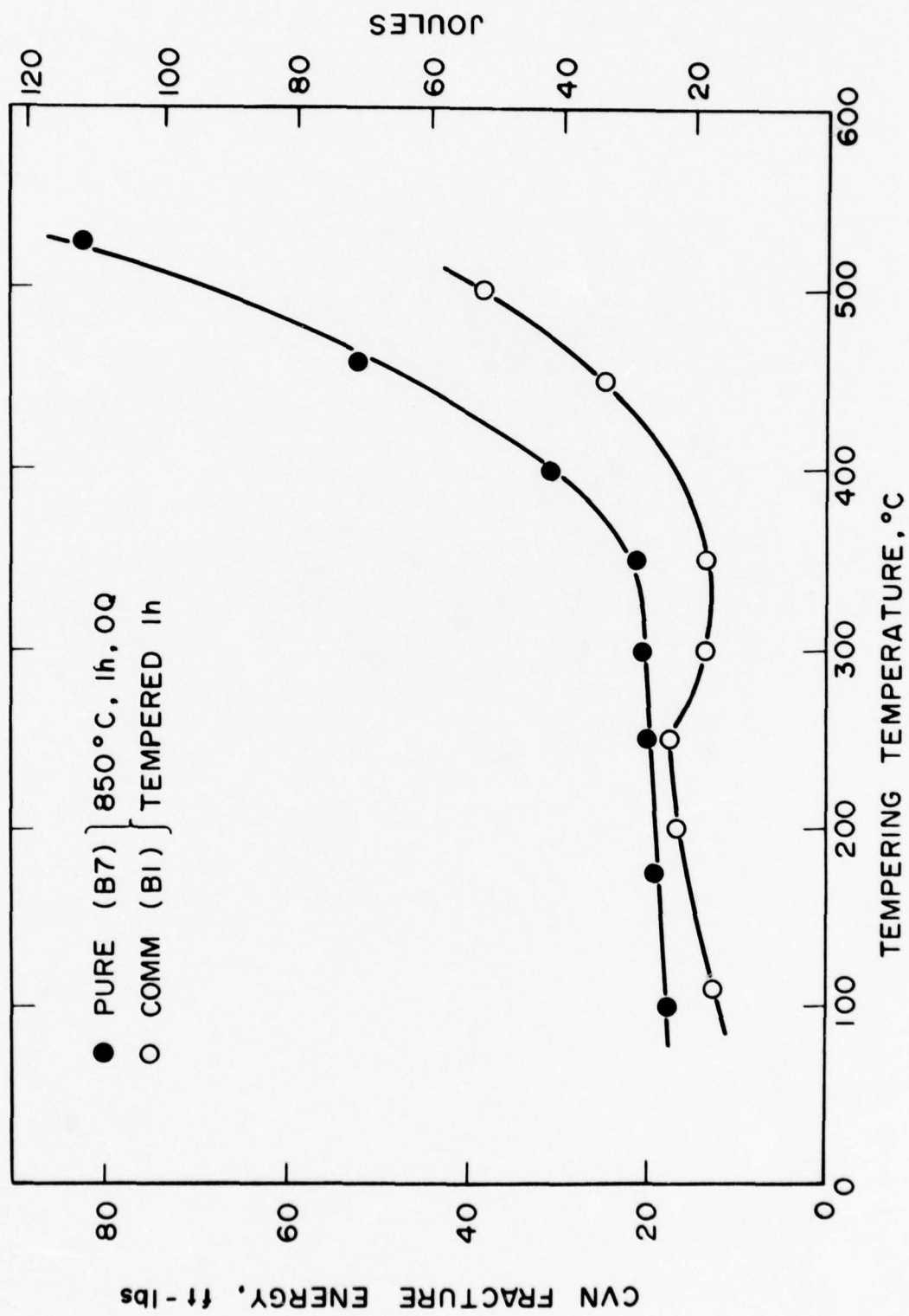
FIG. 10
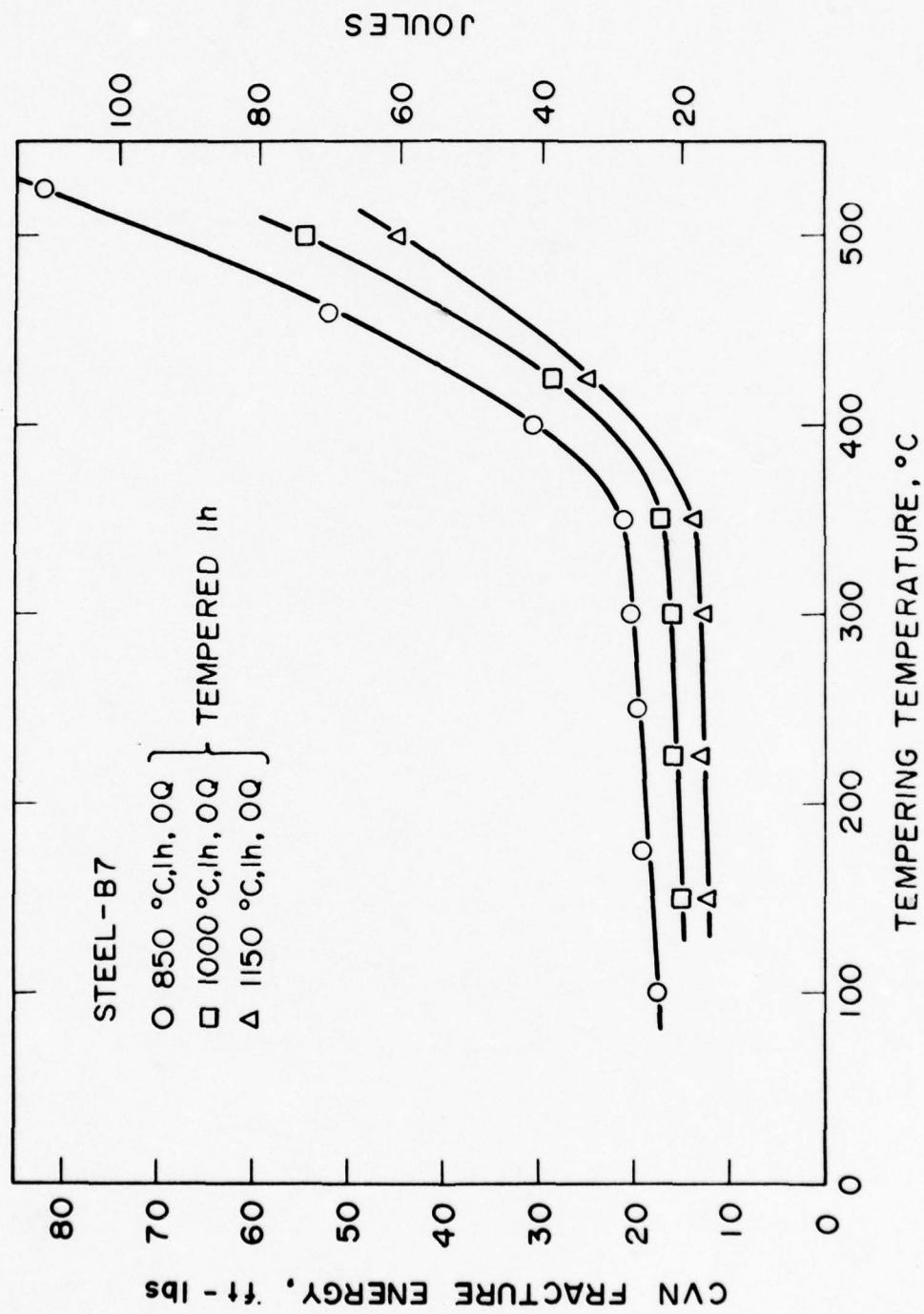
FIG. 11
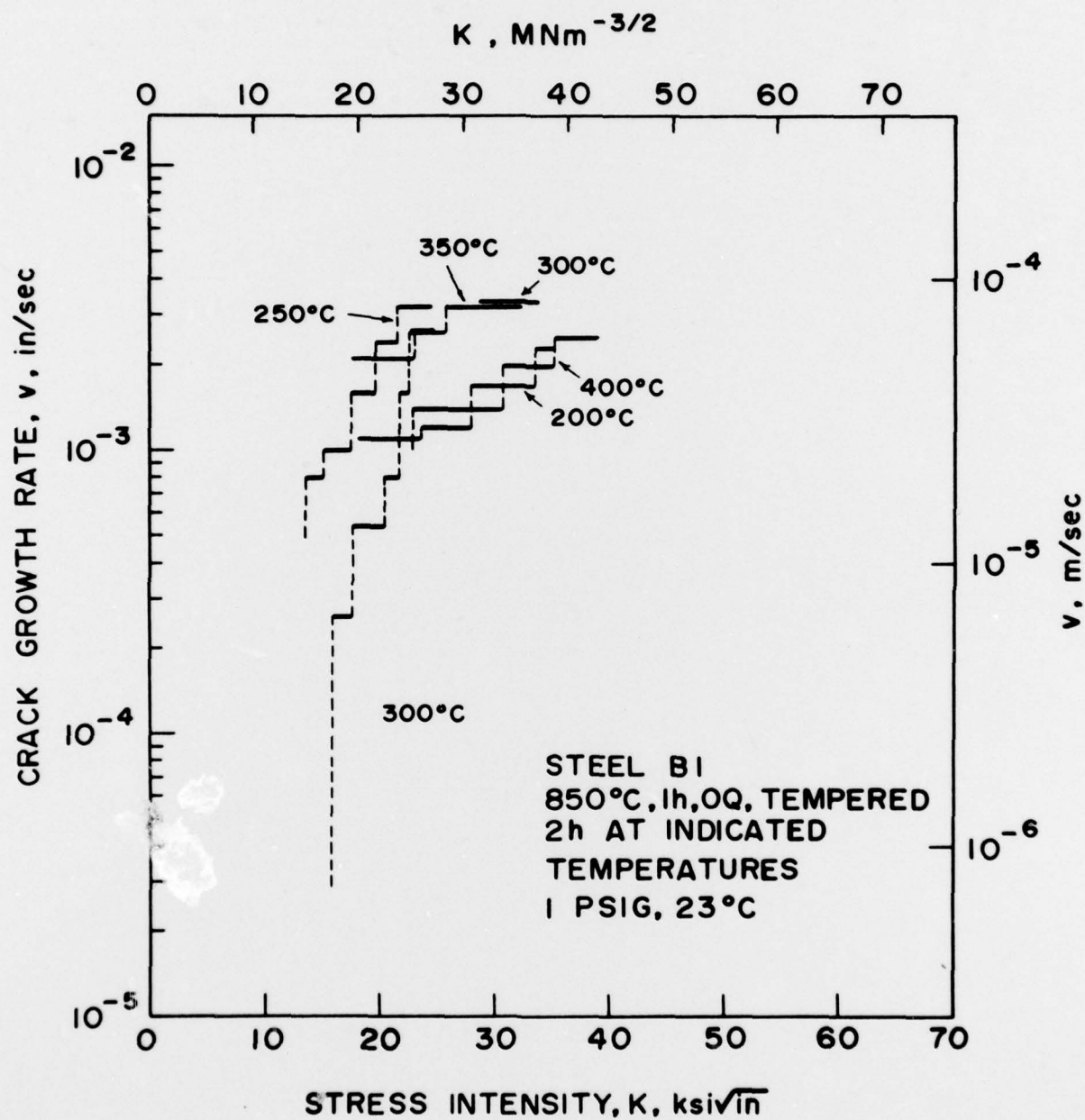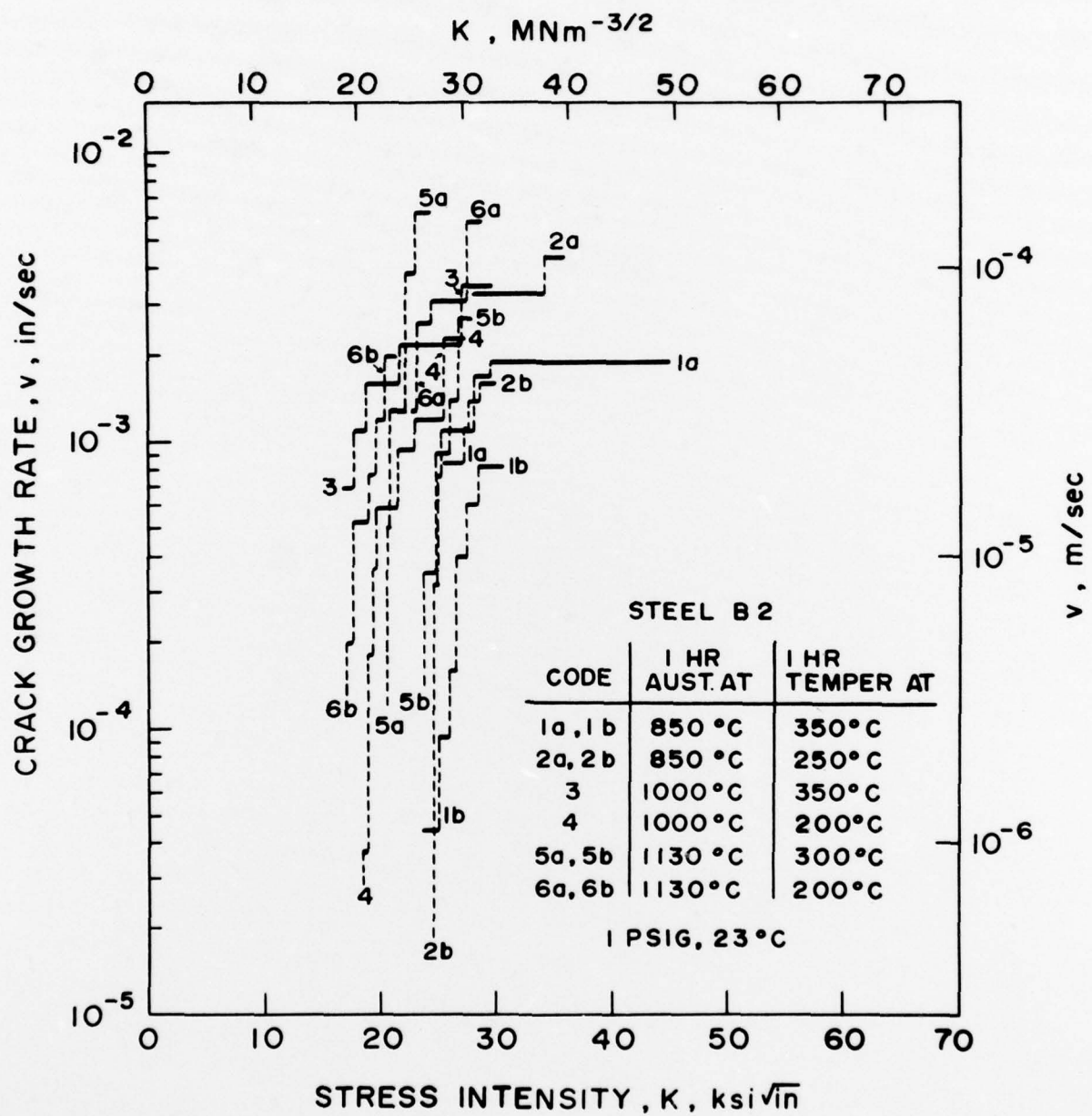
FIG 12

FIG 14

FIG. 13

FIG. 15

FIG. 16

100µ

FIG 17

FIG 184

STEEL- B7 (PURE)
1000°C, 1h, OQ
TEMPERED 350°C, 1h
1 PSIG , 23°C

FIG 18b

FIG. 19

FIG 20

K , MNm$^{-3/2}$

0   10   20   30   40   50   60   70

STEEL B 2

CODE	1 HR AUST. AT	1 HR TEMPER AT
1a, 1b	850 °C	350 °C
2a, 2b	850 °C	250 °C
3	1000 °C	350 °C
4	1000 °C	200 °C
5a, 5b	1130 °C	300 °C
6a, 6b	1130 °C	200 °C

1 PSIG, 23 °C

CRACK GROWTH RATE, v, in/sec

10^{-2}

10^{-3}

10^{-4}

10^{-5}

5a   6a   2a   3   5b   4   6b   4   6a   2b   1a   1a   1b   3   6b   5b   5a   1b   4   2b

v, m/sec

10^{-4}

10^{-5}

10^{-6}

0   10   20   30   40   50   60   70

STRESS INTENSITY, K, ksi$\sqrt{in}$
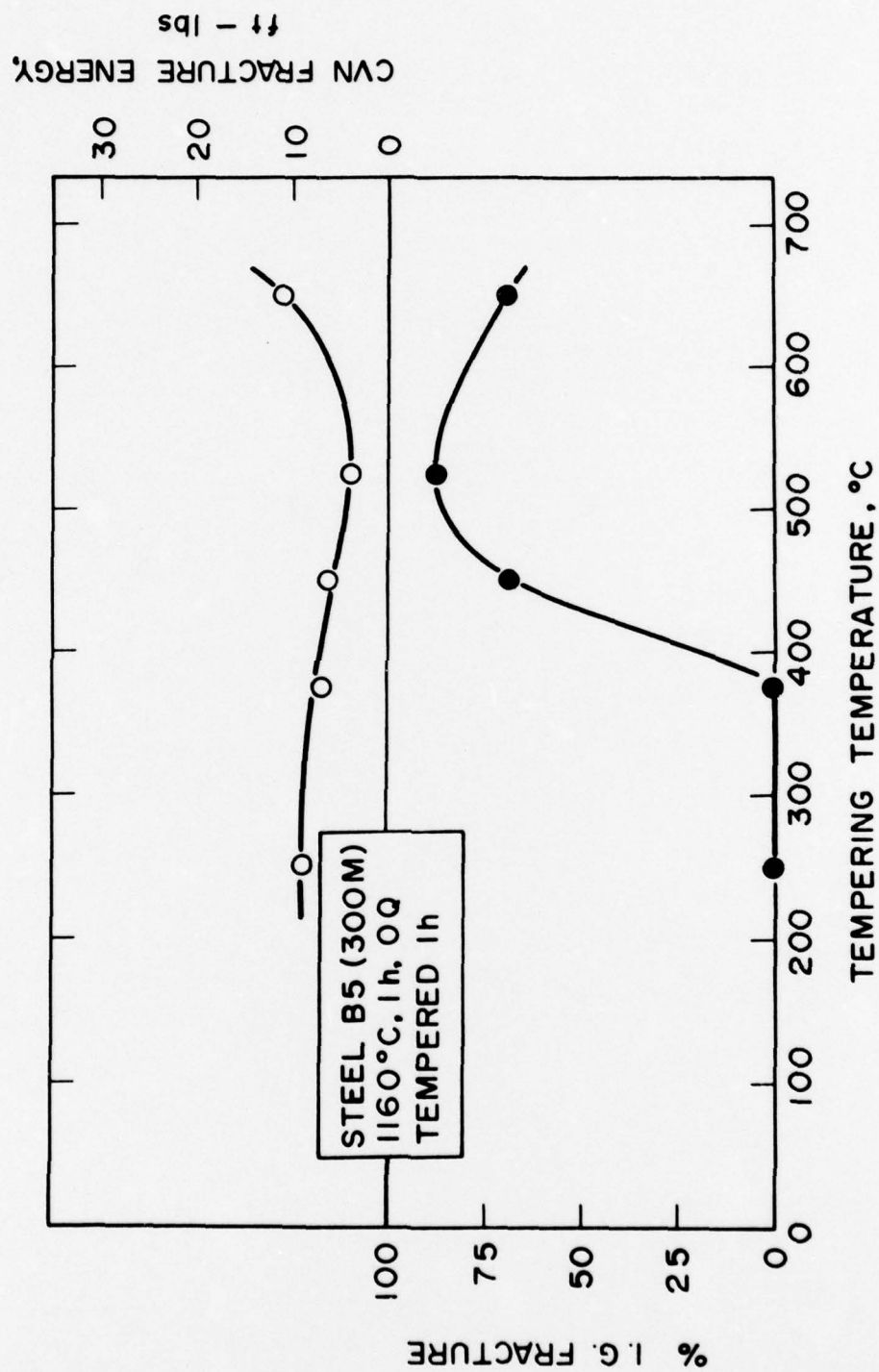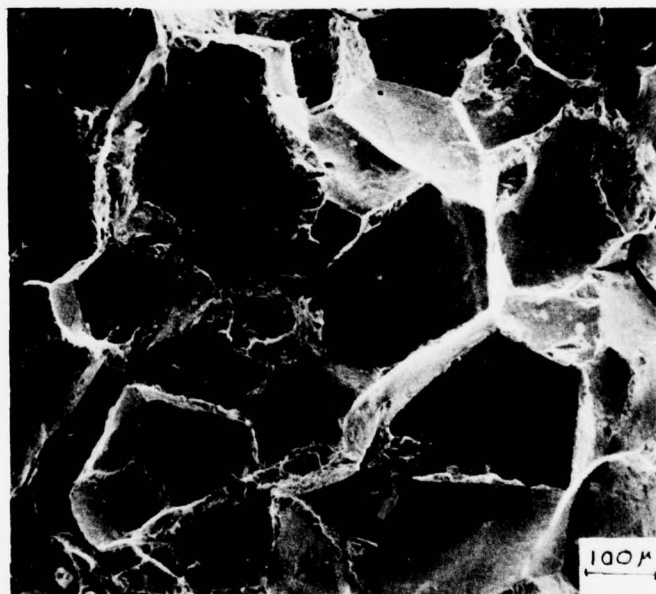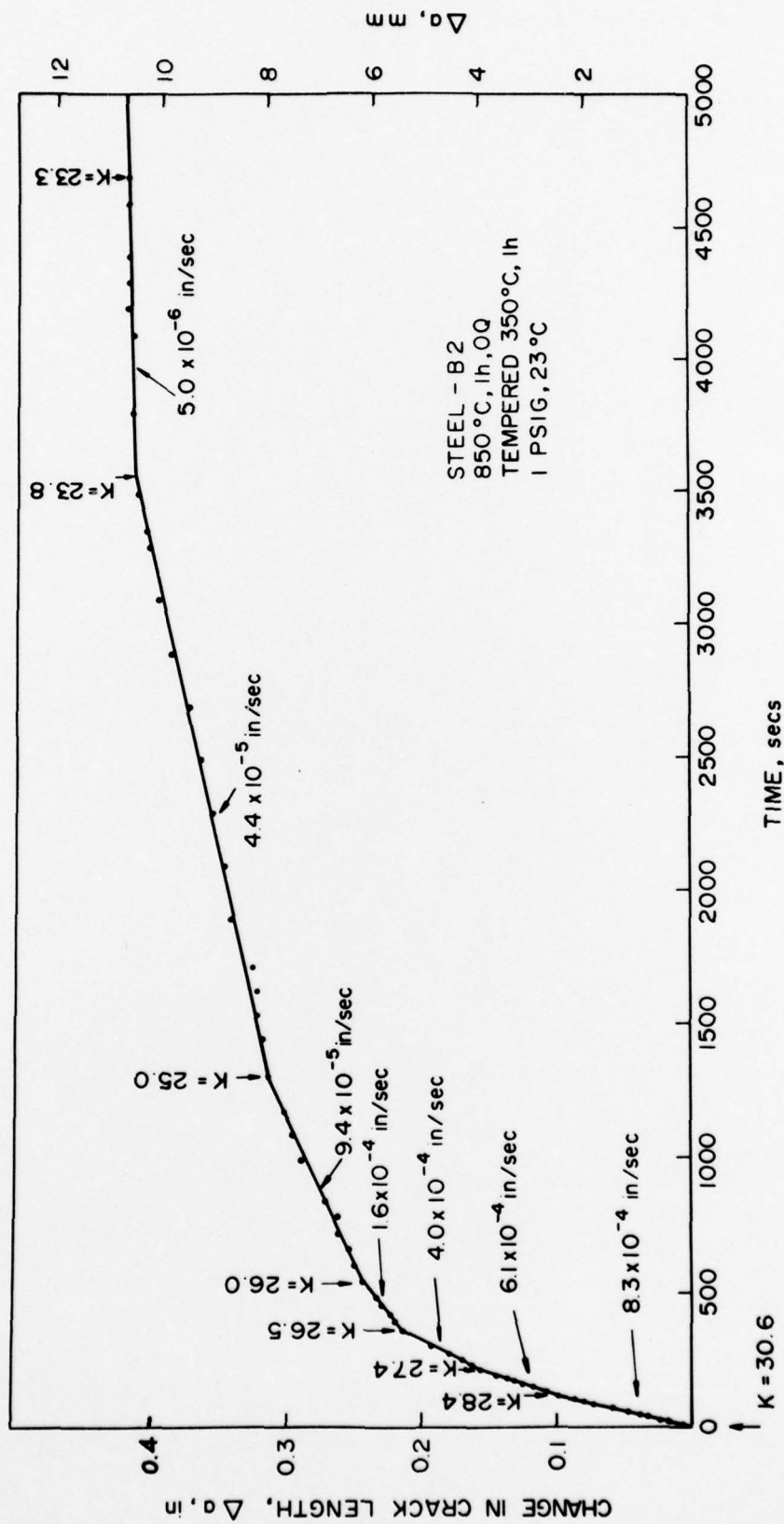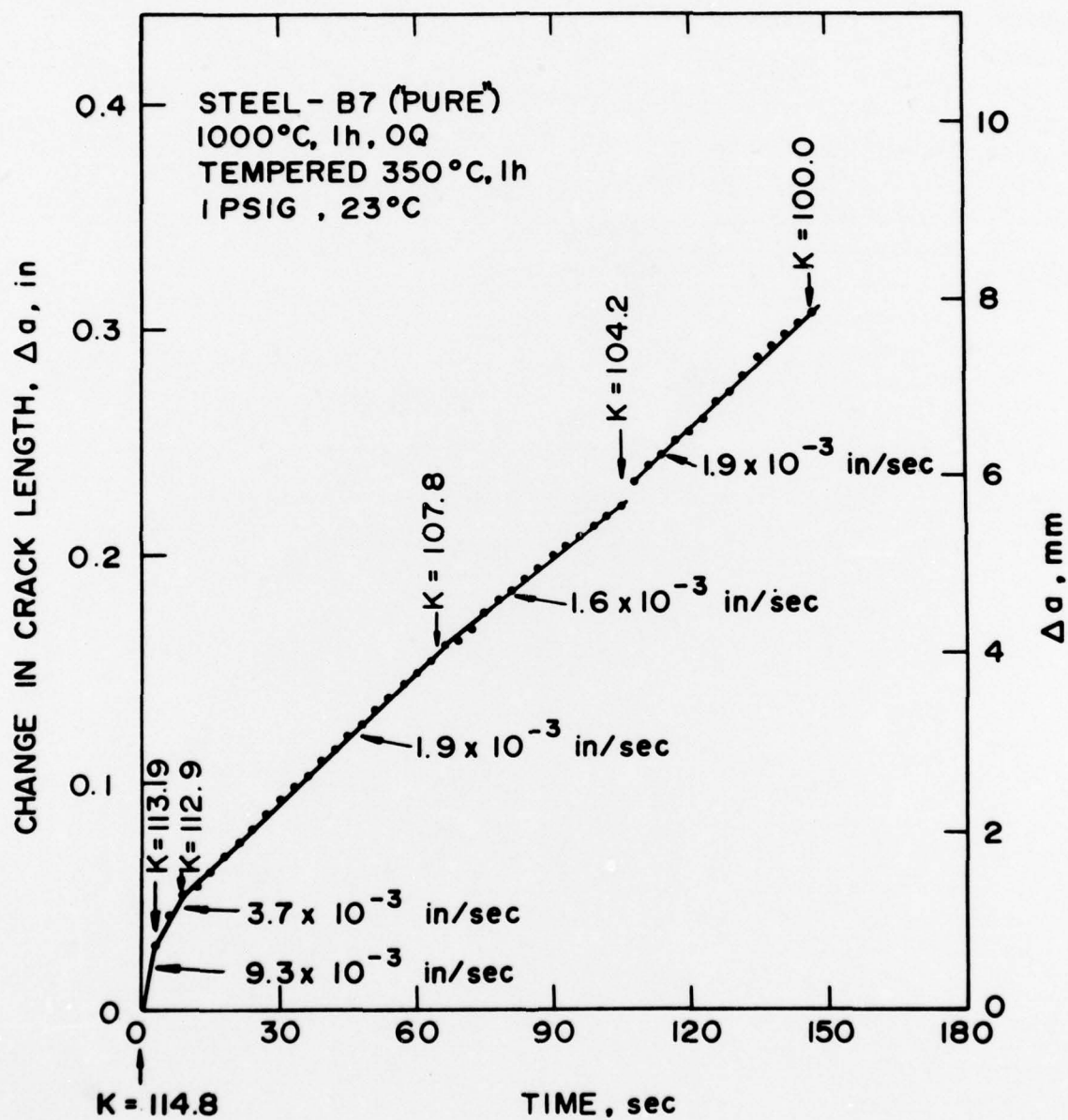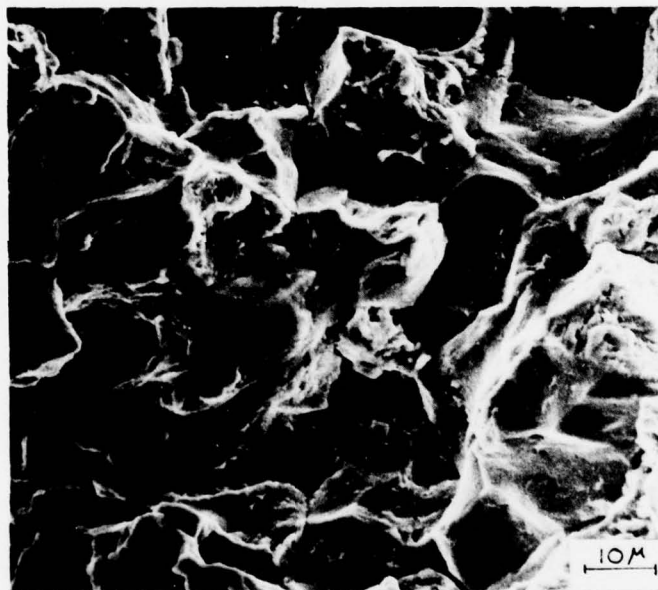
FIG. 21

FIG. 22

FIG. 23

FIG. 24

FIG.25

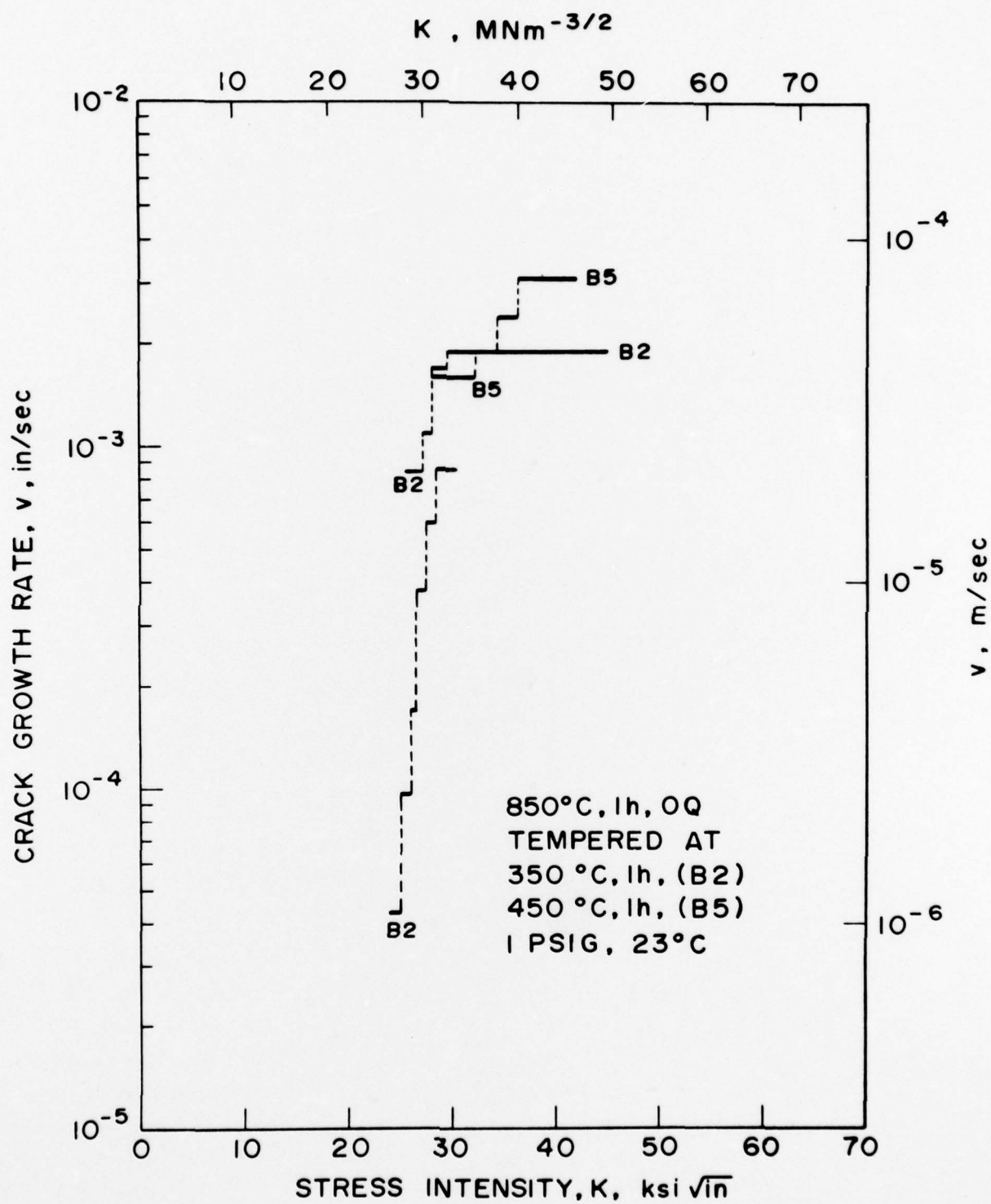K , MNm$^{-3/2}$

850°C, 1h, OQ
TEMPERED AT
350 °C, 1h, (B2)
450 °C, 1h, (B5)
1 PSIG, 23°C

FIG. 26

FIG 27

FIG. 28

FIG. 29